

Computational Modeling for Predicting 3D Cancer Cell Invasion into ECM
 Fiber Network

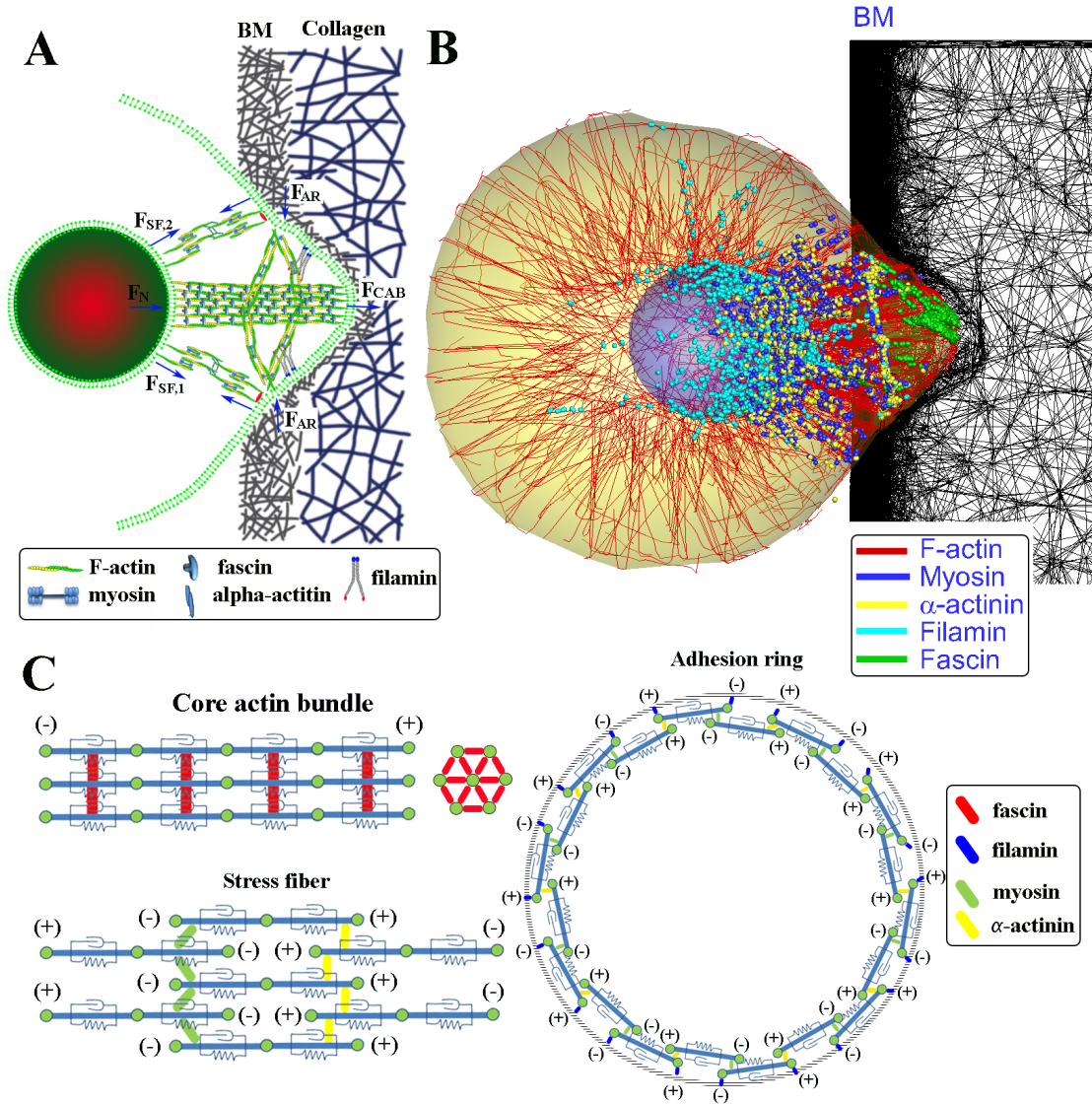


Figure 1. Cancer extravasation model infiltrating into basement membrane (BM) and collagen type 1 network. A) Schematic showing three actin-based structures, such as a core actin bundle (CAB), an adhesion ring (AR), and actin stress fibers (SF). These structures are composed of F-actin, fascin, filamin, myosin, α -actinin. F_{CAB} is CAB force due to actin polymerization of F-actins, F_{AR} is AR force which pull invadopodia membrane, F_{SF} is actin SF force which pull both invadopodia and nuclear membranes, and F_N is resultant force which push the CAB ($F_N = F_{SF,1} + F_{SF,2}$). B) An

example of simulated computational model of cancer cell extravasation into BM and ECM fiber network. Red, blue, yellow, purple, and green lines indicate F-actin, myosin, α -actinin, filamin, and fascin, respectively. C) schematics shows detailed structures of CAB, AR, and SF, here F-actin is modeled as viscoelastic material with a spring and a dashpot. (+) and (-) signs indicate barded-end and pointed-end of F-actin, respectively. Cross-section of CAB is hexagonally packed with < 10 layers and two adjacent F-actins in the CAB are crosslinked by fascin proteins. Cross-section of AR shows multiple compartments. Each compartment is composed of one free F-actin and two attached F-actins on the cellular membrane, here barded-end (+) of free F-actin is connected to barded-end (+) of attached F-actin via α -actinin and pointed-end (-) of free F-actin is connected to pointed-end (-) of attached F-actin via myosin. Similarly, SF has multiple compartment (800 nm) and each compartment is composed of F-actin, α -actinin, and myosin.

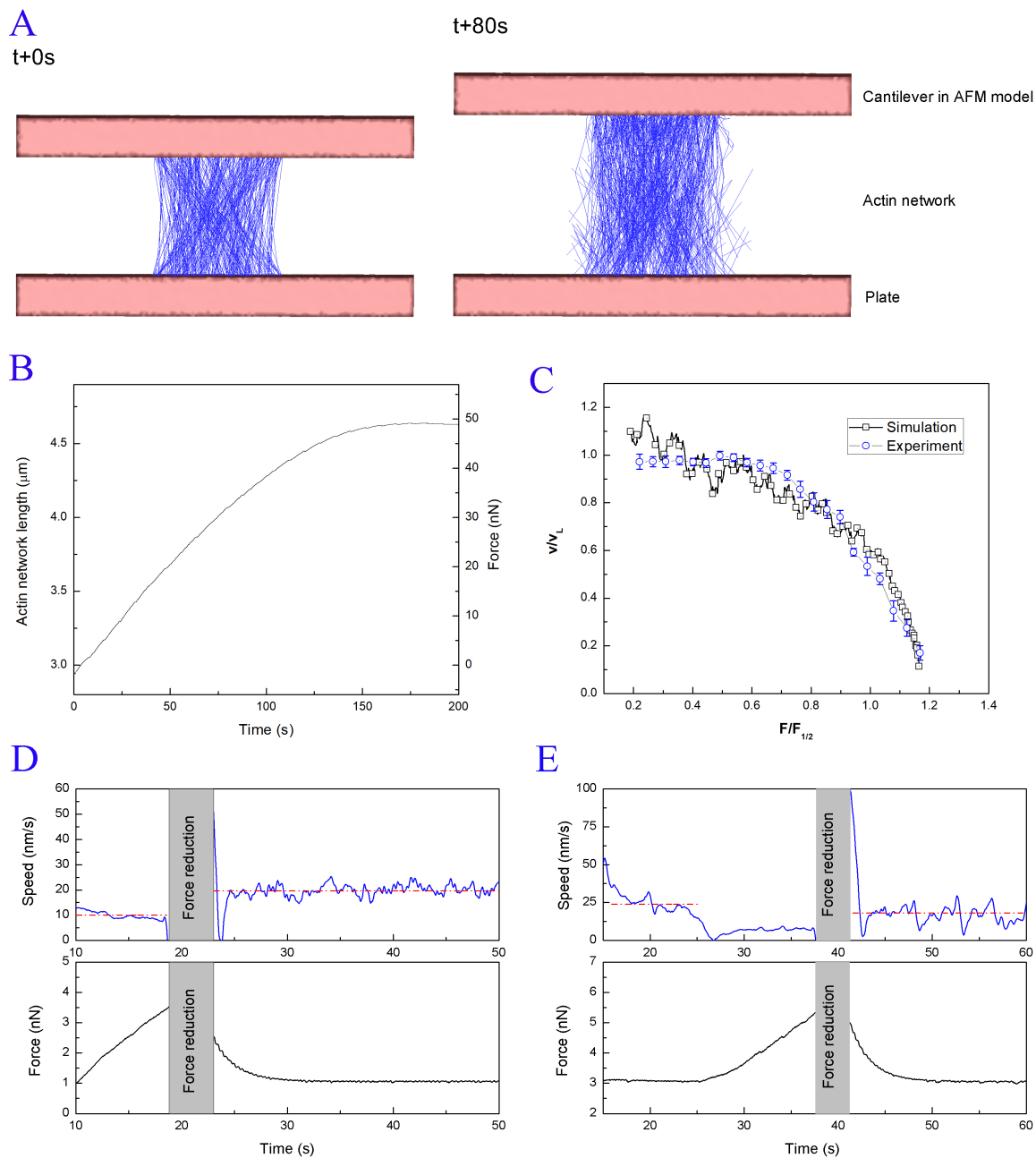


Figure 2. Simulation of growth of actin network model against a flexible cantilever in an atomic force microscope (AFM) system. A) Selective images show initial cubic shape of discrete actin network model ($3.3 \times 3.3 \times 3 \mu m$) which is sandwiched between the plate (bottom) at time-point of 0 s, and a noticeable cantilever deflection by growing actin network at time-point of 80 s. B) A plot showing the length-force of actin network by time. Two growth phases are observed: one is load-independent phase and the other is stall phase. C) Force-velocity relationship for the simulation in B) showing the load-independent and stall phase are compared with existing experimental data (**Error! Reference source not found.**). Values of Force and velocity are normalized by v_L , $F_{1/2}$. D) Actin network was allowed to grow until the load-independent phase was reached, and time-

average growth speed (red dot line) during the load-independent phase was 10.04 nm/s. At time-point of 18s, the force on the network was reduced from 4 nN to 1 nN, and the force was clamped at 1 nN. The time-average growth velocity after the force reduction increased 19.66 nm/s, which is ~1.9 fold faster than the growth velocity at the load independent phase. E) Actin network was initially clamped at 3 nN with average velocity of 23.81 nm/s (red dot line), and then the actin network was allowed to grow naturally until the load-independent phase was reached. Afterwards, the force on the network was reduced from 5.8 nN to 3 nN, and the force was clamped at 3 nN. The time-average growth velocity after the force reduction increased 18.00 nm/s. The simulations shown in A) and B) reproduce experimental observation that demonstrate multiple stable growth velocity for a single force (**Error! Reference source not found.**).

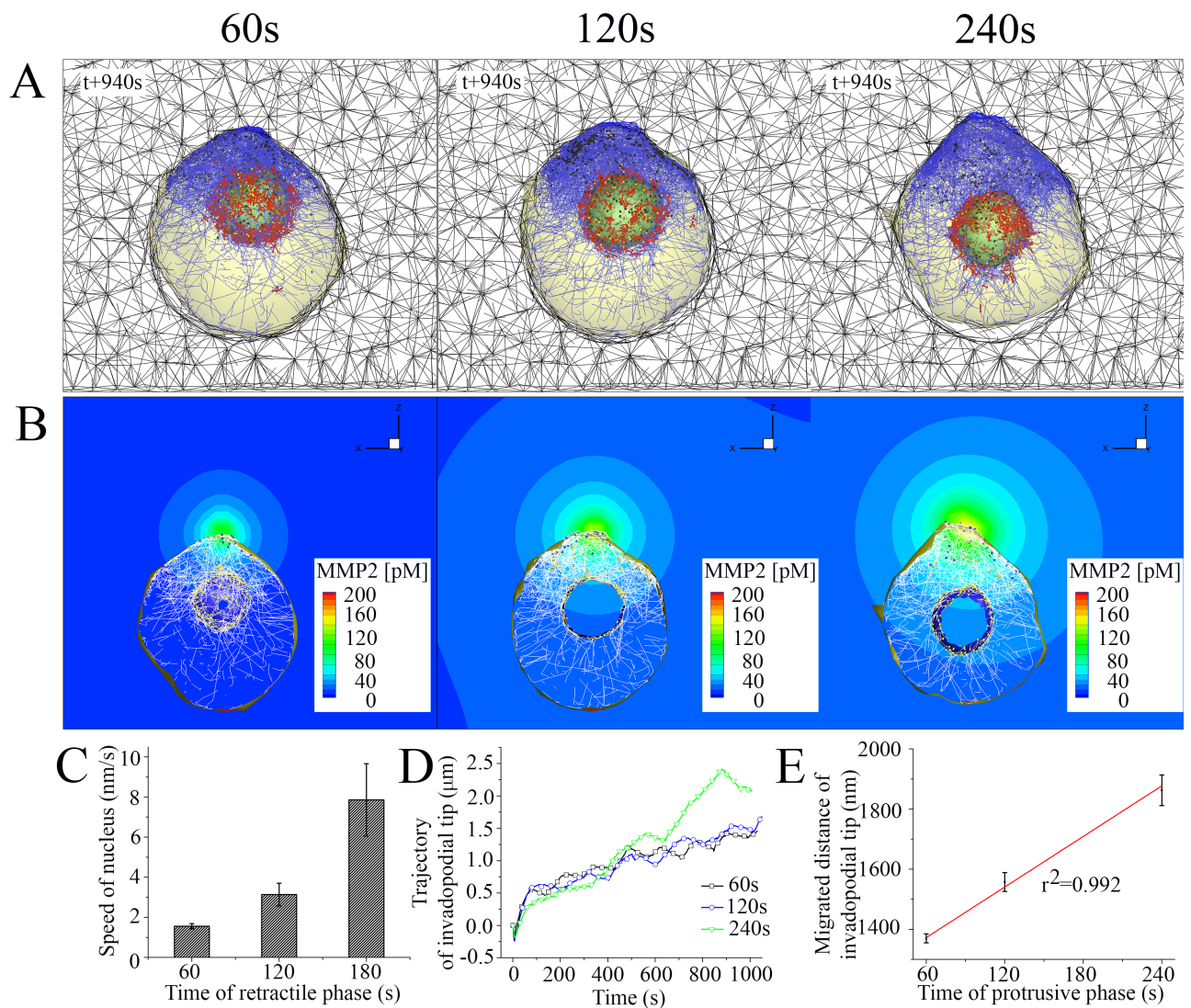


Figure 3. Characterization of invadopodia protrusion dynamics. A) Selected still shots of simulated invadopodia protrusion into ECM under three different duration times in the protrusive phase, such as 60, 120, and 240 s. Blue, red, yellow, dark blue, and black lines indicate F-actin, bipolar myosin filament, α -actinin, filamin, and fascin, respectively. B) Selected MMP-2 contour plots under three different duration times in the protrusive phase, such as 60, 120, and 240 s. C) A graph showing speed of invadopodia versus duration time of retractive phase. D) A graph showing z coordinate of invadopodia tip by time, and E) linear regression ($r^2 = 0.992$) between migrated distance of invadopodial tip and duration time of protrusive phase.

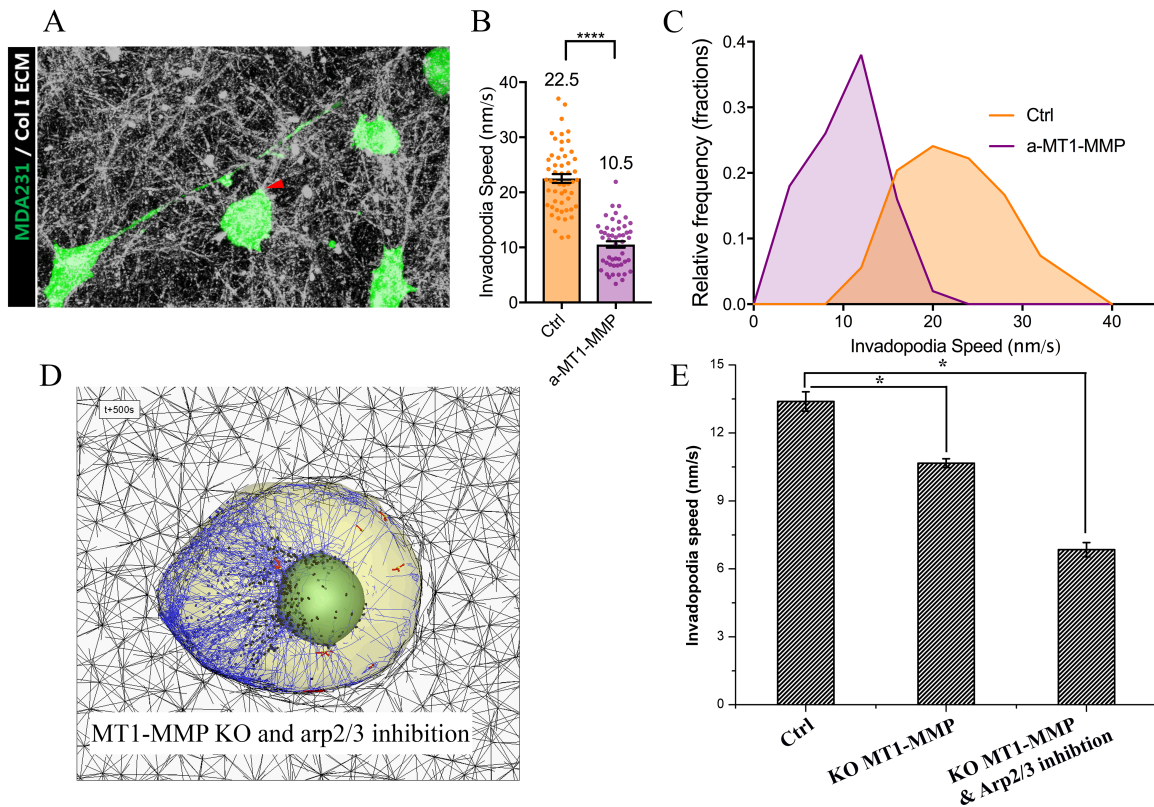


Figure 4. Experimental observation of invadopodia mechanosensing. GFP expressing MDA-MB-231 (MDA231) cells were cultured within a collagen I ECM, and the movement of the invadopodia were imaged and quantified by confocal time-lapse microscopy. A) MDA231 (green) cells cultured in collagen I ECM (white) sends out elongated invadopodia (red arrows) to probe the ECM (scale bar=30 μ m). Quantification (B), mean; C), frequency distribution) of the invadopodia speed from cells treated with antibody against MT1-MMP (a-MT1-MMP) and cells treated with IgG control (Ctrl). For B), data shown are means (displayed above the bar) \pm s.e.m from invadopodia from n=50-54 cells. ****, p<0.0001 from unpaired student t-test. D) A selected still shot of simulated cancer cell with MT1-MMP knockout and Arp2/3 inhibition in ECM fiber network at the time-point of 500s. E) Bar graphs showing time-averaged speeds and s.e.m at the tip of invadopodium for three different cases of Ctrl, KO MT1-MMP only, and KO MT1-MMP and Arp2/3 inhibition. [*P < 0.05, n = 12, 11, 11, one-way ANOVA, posthoc Tukey's test].

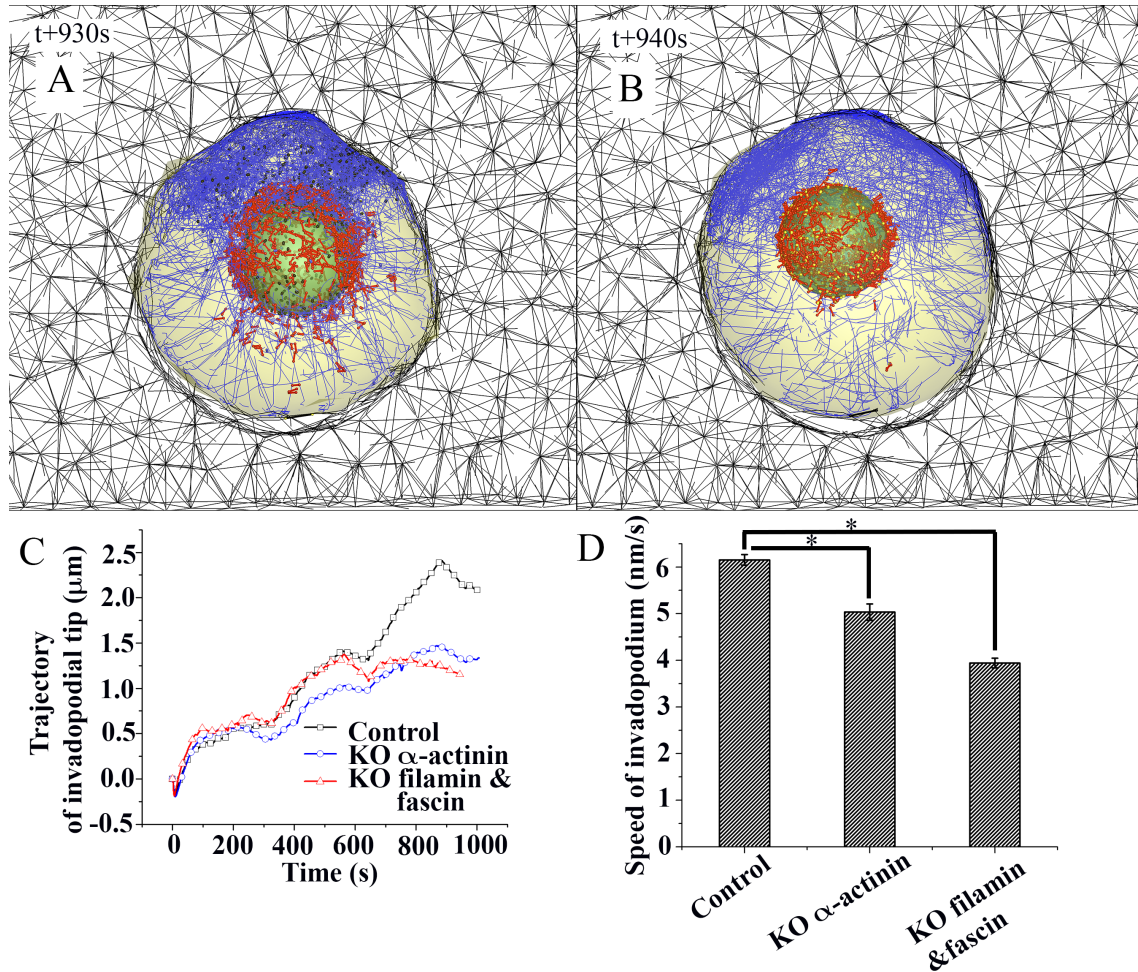


Figure 5. Cancer cell simulations with knockout (KO) of actin-crosslinking molecules. Selected plots of simulation for invadopodia protrusion in ECM with two cases of A) KO α -actinin, and B) KO filamin and fascin. Blue, red, yellow, dark blue, and black lines indicate F-actin, bipolar myosin filament, α -actinin, filamin and fascin, respectively. C) Trajectory of invadopodial tip about three cases of control, KO α -actinin, and KO filamin and fascin. D) Bar graphs showing time-averaged speeds and s.e.m at the tip of invadopodium for three different cases of control, KO α -actinin, and KO filamin and fascin. [*P < 0.05, n = 9, 9, 9, one-way ANOVA, posthoc Tukey's test].

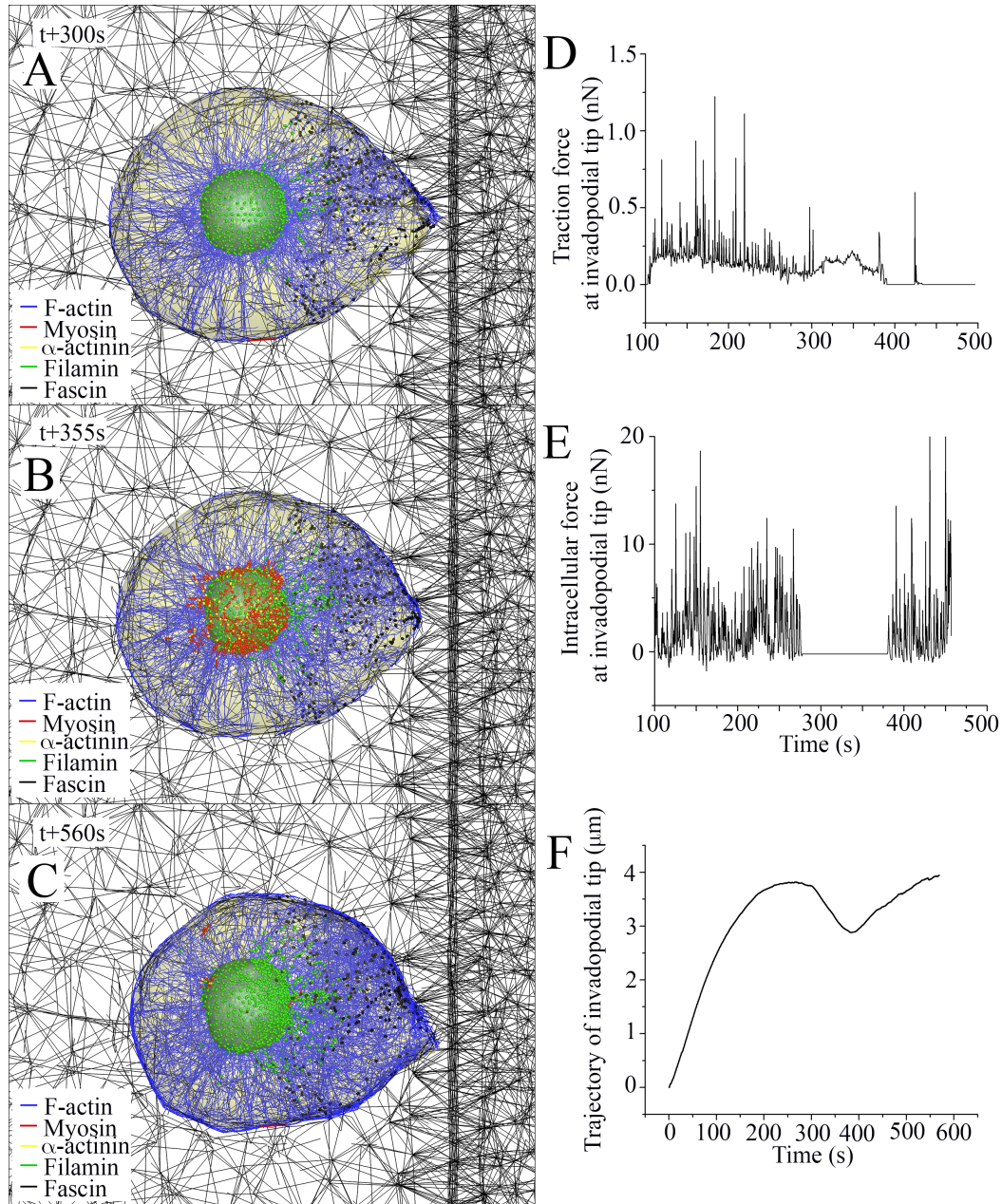


Figure 6. Cyclic motion of invadopodia dynamics during the directed cell migration towards stiffer ECM. Selected still shots of simulated cell migration toward stiffer ECM at time points of A) 300 s (at the end of 1st protrusive phase), B) 355 s (at the end of 1st retractile phase), and C) 560 s (at the end of 2nd protrusive phase). Three graphs in D), E), and F) show time-varying traction (extracellular) force, intracellular force, and trajectory at the tip of invadopodium, respectively.

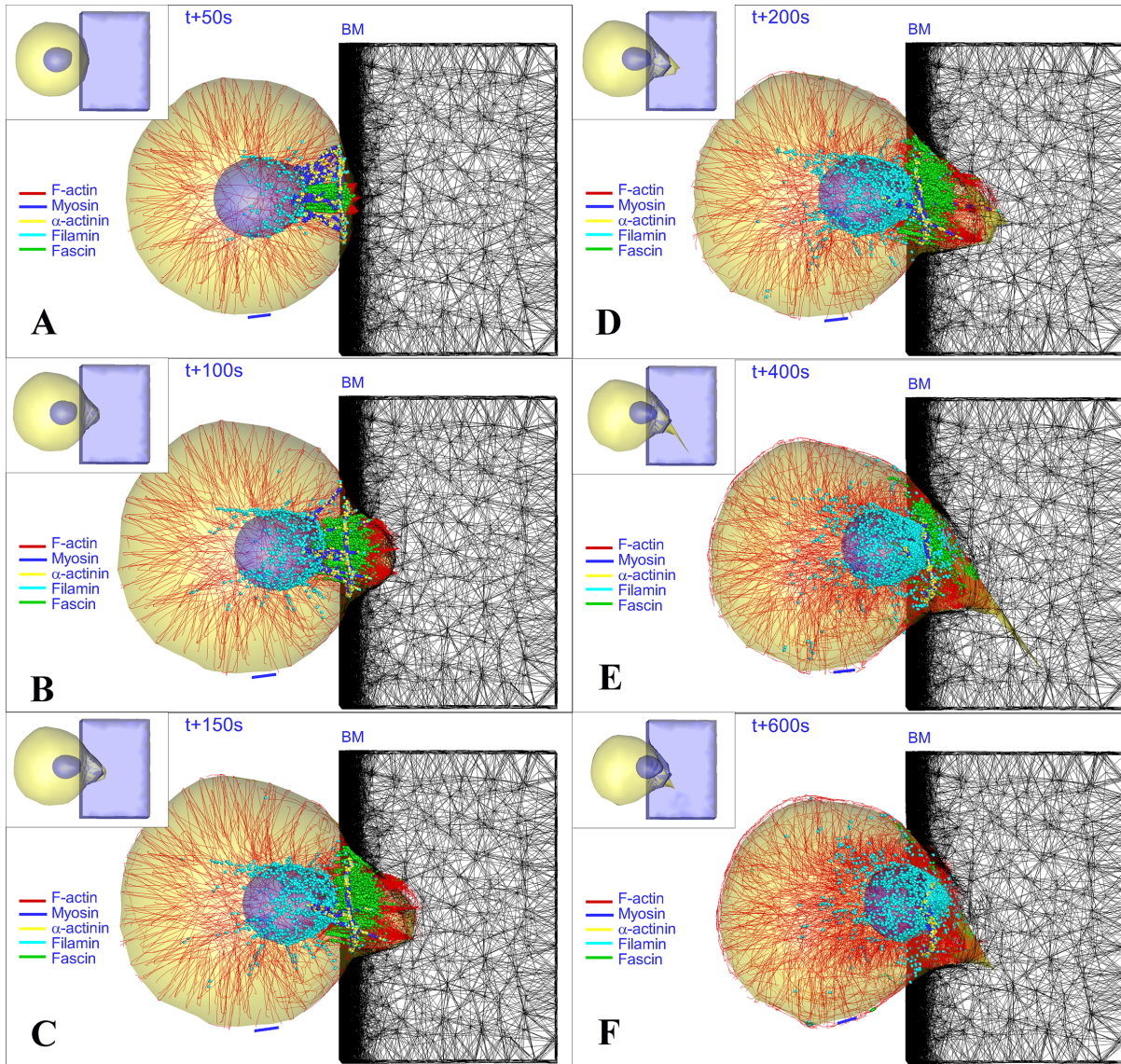


Figure 7. Cancer cell extravasation model infiltrating into BM and ECM fiber network. A) three actin-based structures (CAB, AR, and SFs) were formed at time-point of 50 s, B) invadopodia penetrated through the BM (500 nm) at time-point of 100 s, C) invadopodia further protruded by synergetic actuations of three actin-based structures at time-point of 150 s, D) invadopodia protrusion was maximized at time-point of 200 s, E) the nucleus was pulled toward invadopodia but invadopodia was retracted during the retractile phase at time-point of 400 s, and F) the nucleus was further pulled and penetrating through the BM by contractile motions of bipolar filaments and SFs.

Table 1. Dynamical model of invadopodia protrusion.

Module	Equation	Couplings
CI	$\sum_{j=1}^{n(i)} C_{i,j}^l \left(\frac{dx_i^l}{dt} - \frac{dx_j^l}{dt} \right) + C_1^T \left(\frac{dx_i^l}{dt} - \frac{dx_i^T}{dt} \right) + C_0^l \frac{dx_i^l}{dt} = \mathbf{F}_{E,i}^l + \mathbf{F}_{FC,i}^l + \mathbf{F}_{T,i}^l, i = 1, \dots, N_I$	E, CT, ϕ_2, ϕ_3 and ϕ_4
CT	$\sum_{j=1}^{n(i)} C_{i,j}^T \left(\frac{dx_i^T}{dt} - \frac{dx_j^T}{dt} \right) + C_1^T \left(\frac{dx_i^T}{dt} - \frac{dx_i^l}{dt} \right) + C_1^C \left(\frac{dx_i^T}{dt} - \frac{dx_i^C}{dt} \right) + C_0^T \frac{dx_i^T}{dt} = \mathbf{F}_{E,i}^T + \mathbf{F}_{T,i}^T + \mathbf{F}_{C,i}^T, i = 1, \dots, N_T$	CI and CC
CC	$\sum_{j=1}^{n(i)} C_{i,j}^C \left(\frac{dx_i^C}{dt} - \frac{dx_j^C}{dt} \right) + C_1^C \left(\frac{dx_i^C}{dt} - \frac{dx_i^T}{dt} \right) + C_0^C \frac{dx_i^C}{dt} = \mathbf{F}_{E,i}^C + \mathbf{F}_{C,i}^C + \mathbf{F}_{L,i}^C + \mathbf{F}_{P,i}^C, i = 1, \dots, N_C$	CT and CA
CA	$\sum_{k=j-1}^{j+1} C_{i,j}^A \left(\frac{dx_i^A}{dt} - \frac{dx_k^A}{dt} \right) + C_{i,ARP}^A \left(\frac{dx_{i,j}^A}{dt} - \frac{dx_{k,1}^A}{dt} \right) + C_0^A \frac{dx_{i,j}^A}{dt} = \mathbf{F}_{E,i,j}^A + \mathbf{F}_{br,i,j}^A + \mathbf{F}_{L,i,j}^A + \mathbf{F}_{C,i,j}^A, i = 1, \dots, N_A$	CC and CN
CN	$\sum_{j=1}^{n(i)} C_{i,j}^N \left(\frac{dx_i^N}{dt} - \frac{dx_j^N}{dt} \right) + C_0^N \frac{dx_i^N}{dt} = \mathbf{F}_{E,i}^N + \mathbf{F}_{L,i}^N, i = 1, \dots, N_T$	CA
E	$(2C_{ij}^E + C_0^E) \frac{dx_{ij}^E}{dt} = F_{E,ij}^E + F_{FC,ij}^E + F_{D,ij}^{E0}, i = 1, \dots, N_{fiber}^E$	CI and ϕ_6
RD	$\phi_1 \frac{\partial \phi_1}{\partial t} = \nabla \cdot (D_{\phi_1} \nabla \phi_1) - k_{\phi_1:\phi_2}^{on} \phi_1 \phi_2 + k_{\phi_3:\phi_4}^{on} \phi_3 \phi_4 - k_{\phi_1}^{decay} \phi_1$	E, ϕ_2, ϕ_3 and ϕ_4
	$\phi_2 \frac{\partial \phi_2}{\partial t} = \nabla \cdot (D_{\phi_2} \nabla \phi_2) - k_{\phi_1:\phi_2}^{on} \phi_1 \phi_2 - k_{\phi_2:\phi_3}^{on} \phi_2 \phi_3 + k_{\phi_4}^{off} \phi_4 + \alpha_{\phi_2} (x_{tip}^l) \phi_5$	E, CI, ϕ_1, ϕ_3, ϕ_4 and ϕ_5
	$\phi_3 \frac{\partial \phi_3}{\partial t} = -k_{\phi_2:\phi_3}^{on} \phi_2 \phi_3 + k_{\phi_4}^{off} \phi_4 - k_{\phi_3}^{decay} \phi_3 + \alpha_{\phi_3} (x_{tip}^l) \phi_5$	CI, ϕ_2, ϕ_4 and ϕ_5
	$\phi_4 \frac{\partial \phi_4}{\partial t} = k_{\phi_2:\phi_3}^{on} \phi_2 \phi_3 + k_{\phi_3:\phi_4}^{on} \phi_3 \phi_4 - k_{\phi_4}^{off} \phi_4$	CI, ϕ_2 and ϕ_3
	$\phi_5 \frac{\partial \phi_5}{\partial t} = \nabla \cdot (D_{\phi_5} \nabla \phi_5) - k_{\phi_5}^{decay} \phi_5 + k_{\phi_6}^{deg} \phi_1 \phi_6$	ϕ_1 and ϕ_6
	$\phi_6 \frac{\partial \phi_6}{\partial t} = -k_{\phi_6}^{deg} \phi_1 \phi_6$	E and ϕ_1

* MMP-2 (ϕ_1), TIMP-2 (ϕ_2), MT1-MMP (ϕ_3), a ternary complex of MT1-MMP:TIMP-2:proMMP-2 (ϕ_4), ligands (ϕ_5) (or collagen molecules) and ECM (ϕ_6). The three modules describe the dynamics of the cell (C) and ECM (E) modules and the reaction-diffusion (RD) modules. C module: C is composed of five sub-modules representing the invadopodia membrane (CI), the force transduces layer (CT), the actin cortex layer (CC), branched actin network (CA) and the nuclear membrane dynamics (CN). Detailed explanation of Table 1 can be found in *SI Appendix*.